Temporal decay of Néel order in the one-dimensional Fermi-Hubbard model

A. Bauer, F. Dorfner, and F. Heidrich-Meisner
Department of Physics and Arnold Sommerfeld Center for Theoretical Physics, Ludwig-Maximilians-Universität München, D-80333 München, Germany
(Received 11 March 2015; published 27 May 2015)

Motivated by recent experiments with ultracold quantum gases in optical lattices we study the decay of the staggered moment in the one-dimensional Fermi-Hubbard model starting from a perfect Néel state using exact diagonalization and the infinite-system-size time-evolving-block-decimation method. This extends previous work in which the same problem has been addressed for pure spin Hamiltonians. As a main result, we show that the relaxation dynamics of the double occupancy and of the staggered moment are different. The former is controlled by the nearest-neighbor tunneling rate while the latter is much slower and strongly dependent on the interaction strength, indicating that spin excitations are important. This difference in characteristic energy scales for the fast charge dynamics and the much slower spin dynamics is also reflected in the real-time evolution of nearest-neighbor density and spin correlations. A very interesting time dependence emerges in the von Neumann entropy, which at short times increases linearly with a slope proportional to the tunneling matrix element while the long-time growth of entanglement is controlled by spin excitations. Our predictions for the different relaxation dynamics of the staggered moment and the double occupancy should be observable in state-of-the-art optical lattice experiments. We further compare time averages of the double occupancy to the expectation values in both the canonical and diagonal ensembles, which quantitatively disagree with each other on finite systems. We relate the question of thermalization to the eigenstate thermalization hypothesis.

DOI: 10.1103/PhysRevA.91.053628 PACS number(s): 03.75.Ss, 71.10.Pm, 37.10.Jk

I. INTRODUCTION

The nonequilibrium dynamics of order parameters in quenches from ordered into disordered phases and vice versa has been the topic of many studies, including work on Bose-Einstein condensates [1,2], bosons defined on lattice models [3], and systems with antiferromagnetic order [4,5]. In quantum magnets, the dynamics of the staggered magnetization is a simple yet nontrivial example since the Néel state is never an eigenstate of antiferromagnetic Heisenberg models.

In one spatial dimension, since the spontaneous breaking of a continuous symmetry is prohibited, starting from a state with perfect Néel order, the staggered magnetization is expected to decay to zero under the unitary time evolution with a SU(2)-symmetric Hamiltonian. This problem has been intensely studied for the spin-1/2 XXZ chain [6–14] and one observes a temporal power-law decay of the staggered magnetization to zero for the XX case and indications of an exponential decay to zero in the interacting case [6]. The quantum quench dynamics starting from the Néel state has attracted additional attention since an exact solution for the long-time asymptotic behavior could be obtained by exploiting the integrability of the model [9,12,13]. Therefore, the question of whether the steady state in this quench problem can be described by the generalized Gibbs ensemble [15] could be addressed with rigor.

In the context of condensed-matter experiments, the decay of Néel order is related to time-resolved spectroscopy with Mott insulators in real materials [16–18]. In experiments with ultracold quantum gases, it is often particularly easy to prepare initial real-space product states with a high fidelity, which has been used as the starting point in several nonequilibrium studies of Hubbard- and Heisenberg-type models [19–23]. The particular problem of the decay of Néel order has so far been addressed in the noninteracting case in one dimension [24] (where the initial state is an ideal charge density wave state of one spin component) and for a two-dimensional system [25]. Moreover, the decay of a spin spiral has been investigated in a two-component Bose gas in the strongly interacting regime, where it can be described by the Heisenberg model, in one and two dimensions [26]. The reverse problem, namely the formation of antiferromagnetic order in time-dependent protocols, is of equal relevance since this may provide a path for studying magnetic order in the quantum regime in ultracold atomic gas experiments [27–31], which has been the goal of a series of recent experiments [32–36]. For other nonequilibrium experiments with fermions in optical lattices, see Refs. [37–39].

In this work, we study the real-time decay of the Néel state in the one-dimensional Fermi-Hubbard model, which, first, extends previous studies [6] by incorporating charge dynamics and, second, is motivated by two related recent experiments with fermions in one dimension [24] and bosons in two dimensions [25]. The Hamiltonian reads

$$H = -t_0 \sum_i (c^\dagger_{i+1,\sigma} c_{i,\sigma} + \text{H.c.}) + U \sum_i n_{i\uparrow} n_{i\downarrow}, \qquad (1)$$

where t_0 is the hopping matrix element, U is the on-site repulsion, $c^\dagger_{i,\sigma}$ creates a fermion with spin $\sigma = \uparrow,\downarrow$ on site i, and $n_{i\sigma} = c^\dagger_{i,\sigma} c_{i,\sigma}$. The initial state is given by

$$|\psi_0\rangle = |\ldots, \uparrow, \downarrow, \uparrow, \downarrow, \uparrow, \downarrow, \ldots\rangle. \qquad (2)$$

Consequently, we are at half filling. We use the infinite-system-size time-evolving block-decimation (iTEBD) algorithm [40] to compute the time dependence of several observables such as the staggered magnetization, the double occupancy, nearest-neighbor correlations, and the von Neumann entropy (we set $\hbar = 1$). As a main result, we demonstrate that the relevant time scales for the relaxation of the double occupancy is

set by the inverse of the hopping matrix element $1/t_0$ while for the staggered magnetization and nearest-neighbor spin correlations, the dynamics is the slower the larger U is. The difference in the relaxation dynamics can most clearly be discerned in the strongly interacting regime $U/t_0 > 4$. This reflects the existence of two characteristic velocities in the low-energy, equilibrium physics of strongly interacting one-dimensional (1D) systems, namely the spin and charge velocity, related to spin-charge separation [41]. Furthermore, there are fingerprints in the time dependence of the entanglement entropy. In general, in global quantum quenches, one expects a linear increase of $S_{\mathrm{vN}}(t) \sim t$ in time [42–44]. In our case, we observe a short-time dynamics governed by charge excitations where $S_{\mathrm{vN}} \sim t_0 t$ while at longer times $S_{\mathrm{vN}} \propto t/U$, suggesting that spin excitations are relevant for which the energy scale is the magnetic exchange constant $J = 4t_0^2/U$.

Furthermore, we analyze the dependency of the double occupancy on the postquench values of U/t_0 and we investigate whether the steady-state values are thermal or not. The latter is a possible scenario for an integrable 1D model [15]. We observe that time averages are close to the expectation values in the diagonal ensemble [45], while on the system sizes accessible to exact diagonalization, the expectation values in the diagonal and canonical ensemble are clearly different. In this context, we also show that the distribution of eigenstate expectation values is in general broad, in contrast to systems that are expected to thermalize in the framework of the eigenstate thermalization hypothesis [45–47]. The observation of broad eigenstate expectation values of observables in our model is similar to those of Refs. [48,49] made for integrable models of interacting spinless fermions. For other recent studies of interaction quantum quenches in the one-dimensional Fermi-Hubbard model, see Refs. [50–55], and for studies of the time evolution starting from a perfect Néel state in higher dimensions, see Refs. [4,5,56]. The nonequilibrium dynamics starting from this particular state yet combined with a sudden expansion into a homogeneous empty lattice has been investigated in Ref. [57].

The plan of this paper is the following. We provide a brief overview over the numerical methods and definitions in Sec. II. Section III contains our main results, discussing the time evolution of observables and von Neumann entropy, steady-state values, thermalization, and the dynamics in the strongly interacting regime. We conclude with a summary presented in Sec. IV.

II. NUMERICAL METHODS

In this work we use two wave-function-based methods, exact diagonalization (ED) and the iTEBD method, to study nonequilibrium dynamics in the Fermi-Hubbard model. We further use a standard density matrix renormalization group (DMRG) code to compute ground-state expectation values [58,59].

A. iTEBD

We use Vidal's iTEBD algorithm for infinite systems to calculate the time evolution of the observables of interest starting from the perfect Néel state. This method approximates the true wave function by a matrix-product state ansatz [60] appropriate for the thermodynamic limit and is related to time-dependent density matrix renormalization group methods [61,62] and time-evolving block decimation (TEBD) for finite systems [63]. We use a Trotter-Suzuki breakup of the time-evolution operator with a time step that is chosen small enough to resolve high-frequency oscillations at large U/t_0. The maximum number of states is bounded by $\chi_{\max} = 1024$. We compared runs with different $\chi_{\max}$ and show only data for which the results are indistinguishable on the scale of the figures.

Compared to its siblings—the time-dependent density matrix renormalization group method [61,62] and TEBD [63]—the advantage of iTEBD is clearly that it is set up directly for the thermodynamic limit. Moreover, both TEBD and iTEBD are particularly well suited for problems in which the initial state has an exact matrix-product state representation, which applies to our situation. All theses approaches rely on approximating the time-evolved wave function through matrix-product states which only gives a faithful representation if the time-evolved wave function does not encode a large amount of entanglement [60]. While our initial state is not entangled, the entanglement in a global quantum quench like ours grows linearly in time (see, e.g., Ref. [42]), which results in an exponential increase of computational effort [60]. Thus, as the time evolution progresses, eventually, going from time step t to $t + \Delta t$ will consume more computational time than the whole previous calculation. By keeping the discarded weight constant in every step, one accounts for the time-dependent increase of the entanglement entropy, and by carrying out simulations with a different discarded weight the accuracy of the data can be controlled. While the linear increase of the entanglement entropy with time is generic to a global quantum quench, the actual quench, model parameters, and the observable determine the actual numerical costs such that no general prediction of numerical effort and accuracy is possible.

B. Exact diagonalization

Our second method is exact diagonalization. We perform the time evolution in a truncated Krylov space (see Ref. [64] for a review and references). To be able to treat larger systems we exploit symmetries of the Hamiltonian (1), namely conservation of total particle number N, total spin S^z, invariance under lattice translations (quasimomentum k), the parity, and spin-flip symmetry. In ED simulations, we use periodic boundary conditions, and the number of sites is denoted by L.

C. Observables

Key quantities in our analysis are the double occupancy

$$d(t) = \frac{1}{L}\sum_{i=1}^{L}\langle n_{i\uparrow}n_{i\downarrow}\rangle, \tag{3}$$

where the associated operator is $\hat{d} = \frac{1}{L}\sum_{i=1}^{L} n_{i\uparrow}n_{i\downarrow}$. The staggered magnetization is

$$m_s(t) = \frac{1}{2L}\sum_{i=1}^{L}(-1)^i\langle n_{i\uparrow} - n_{i\downarrow}\rangle. \tag{4}$$

We further study nearest-neighbor density and spin correlations defined as $N_i = \langle n_i n_{i+1}\rangle$ and $S_i = \langle S_i^z S_{i+1}^z\rangle$, with $n_i = n_{i\uparrow} + n_{i\downarrow}$ and $S_i^z = (n_{i\uparrow} - n_{i\downarrow})/2$. The von Neumann entropy for a central cut through the system is computed from

$$S_{\rm vN} = -{\rm tr}[\rho_A \ln \rho_A], \tag{5}$$

where ρ_A is the reduced density matrix of one half of the system.

III. RESULTS

A. Time evolution and characteristic time scales

1. Double occupancy and staggered moment

Figures 1(a) and 1(b) show the time evolution of the double occupancy $d(t)$ and of the staggered magnetization $m_s(t)$, respectively, obtained from iTEBD simulations. While the double occupancy rapidly approaches a time-independent regime for all values of U/t_0 considered here, the relaxation of the staggered magnetization towards $m_s = 0$ is much slower. It is very instructive to replot $m_s(t)$ versus t/U [inset in Fig. 1(b)]. This results in a collapse of the data for $U > 4t_0$, which is the better the larger U/t_0 is. Therefore, the relaxation of double occupancy and staggered magnetization occur at different time scales $1/t_0$ and U, respectively. This suggests that the relaxation of spin-related quantities is set by the magnetic exchange matrix element given by $J = 4t_0^2/U$ for large U/t_0. Both quantities further exhibit coherent oscillations that decay during the approach to a stationary value. For the double occupancy the frequency is given by $\omega = U$ for large $U \gg t_0$. By contrast, the period of oscillations in $m_s(t)$ increases in the large-U/t_0 limit. This is expected, since in the Heisenberg limit the period of oscillations is $1/(2J)$ with $J = 4U/t_0^2$ [6]. Note that the noninteracting case has recently been studied comprehensively in Ref. [65] and that our iTEBD results agree with the analytical solution for the $U = 0$ case [6,66,67].

The short-time dynamics of both quantities ($\hat{O}$ representing an observable) can be obtained analytically by expanding the time-evolution operator:

$$\langle \hat{O}(t)\rangle \approx \langle\psi_0|\hat{O}|\psi_0\rangle + i\langle\psi_0|[H,\hat{O}]|\psi_0\rangle t - \tfrac{1}{2}\langle\psi_0|[H,[H,\hat{O}]]|\psi_0\rangle t^2 + \mathcal{O}(t^3). \tag{6}$$

For both double occupancy and staggered magnetization, the leading time dependence is $\sim t^2$ and comes from $\langle\psi_0|H\hat{O}H|\psi_0\rangle \propto t_0^2$, which is independent of U. Hence, the nontrivial U dependence cannot be deduced from this short-time dynamics. Second-order time-dependent perturbation theory in t_0/U gives

$$d(t) = \frac{8t_0^2}{U^2}\sin^2\left(\frac{Ut}{2}\right), \tag{7}$$

$$m_s(t) = \frac{1}{2} - \frac{8t_0^2}{U^2}\sin^2\left(\frac{Ut}{2}\right). \tag{8}$$

These expressions agree with our numerical data for $U/t_0 \gtrsim 16$.

2. Comparison to Heisenberg model

For completeness, we show that the time dependence of the staggered magnetization in the large-U/t_0 limit approaches the one of the spin-1/2 Heisenberg model $H = J\sum_i \vec{S}_i \cdot \vec{S}_{i+1}$, where J is the magnetic exchange coupling. We expect the time evolution of $m_s(t)$ to be identical in both models in the limit of large U/J since the Heisenberg model is derived from the Fermi-Hubbard model via a Schrieffer-Wolff transformation that projects onto the subspace of vanishing double occupancy [68].

The comparison is shown in Fig. 2, where we present iTEBD results for $U/t_0 = 16,32$ and the pure spin system. We see that the results for the two models become quantitatively similar for large U/t_0. Moreover, the short-time dynamics in $m_s(t)$, namely the small initial oscillations (see the arrow

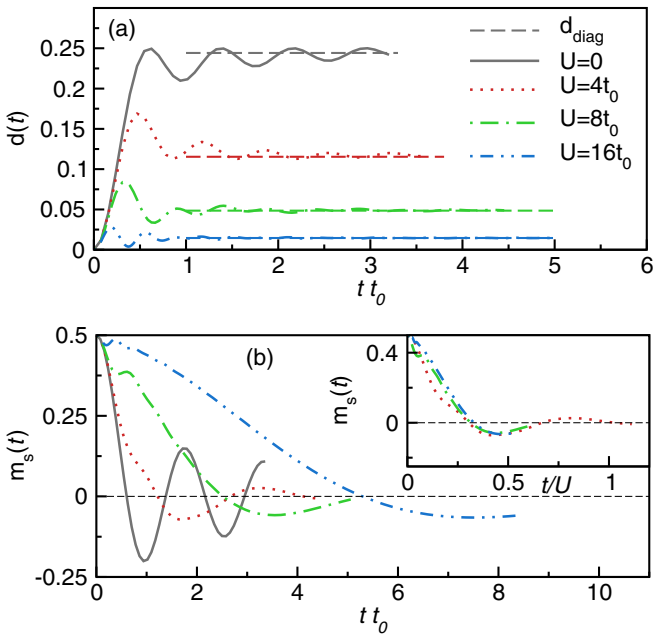

FIG. 1. (Color online) (a) Double occupancy $d(t)$ and (b) staggered magnetization $m_s(t)$ as a function of time during the quench from the Néel state to $U/t_0 = 0,4,8,16$ (iTEBD data). Dashed lines in (a), expectation value $d_{\rm diag}$ in the diagonal ensemble Eq. (10) from ED ($L = 10$). Inset in (b), $m_s(t)$ plotted versus t/U for $U/t_0 = 4,8,16$.

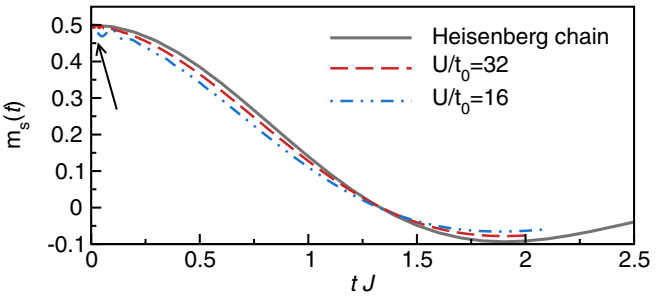

FIG. 2. (Color online) Time dependence of the staggered moment for Heisenberg (solid line) and Hubbard model with a large $U/t_0 = 16,32$ (iTEBD data), plotted versus time measured in inverse units of the magnetic exchange constant $J = 4t_0^2/U$. The arrow indicates the small-amplitude oscillations in the short-time dynamics for finite $U/t_0 < \infty$ whose frequency is given by U.

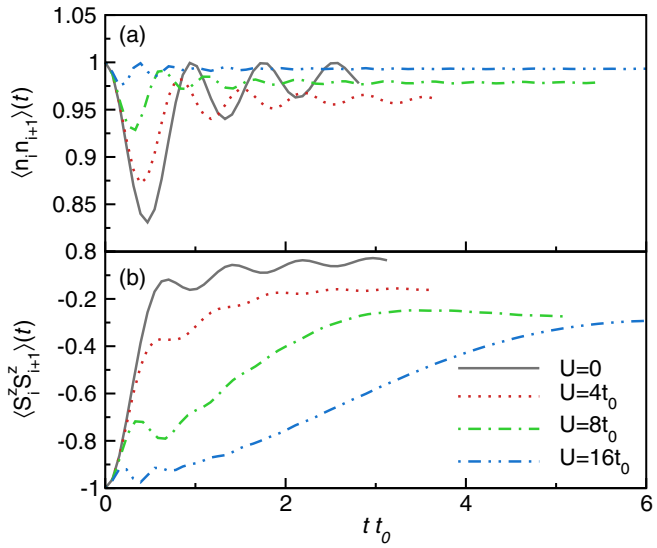

FIG. 3. (Color online) (a) Nearest-neighbor charge correlations $N_i(t) = \langle n_i n_{i+1}\rangle$ and (b) nearest-neighbor, longitudinal spin correlations $S_i(t) = \langle S^z_i S^z_{i+1}\rangle$ as a function of time for $U/t_0 = 0,4,8,16$ (iTEBD results).

in the figure), disappear as U/t_0 increases, indicating the complete suppression of short-time charge dynamics. This is accompanied by a shrinking of the time window in which the short-time dynamics is governed by $\delta m_s(t) = m_s(t) - m_s(t = 0) \propto (t_0 t)^2$ [see Eq. (6)], which gets replaced by $\delta m_s(t) \propto (Jt)^2$ (the latter follows from considering the Heisenberg model).

3. Nearest-neighbor correlations

The time dependence of nearest-neighbor density correlations $N_i(t)$ [Fig. 3(a)] and spin correlations $S_i(t)$ [Fig. 3(b)] bears similarities to that of the double occupancy and the staggered moment, respectively. The density correlator undergoes a rapid decrease towards a stationary state that happens during the first tunneling time and then exhibits oscillations with a U-dependent frequency. On the contrary, the relaxation dynamics of the spin correlator is much slower, and again controlled by U [the data for $S_i(t)$ can be collapsed in the $U/t_0 > 4$ regime by plotting them versus t_0/U, analogous to the staggered moment].

4. Von Neumann entropy

The existence of two different time scales for the relaxation dynamics of the double occupancy and the staggered magnetization translates into an interesting time dependence of the von Neumann entropy (see Fig. 4). At short times $t \lesssim 0.5/t_0$, $S_{\rm vN} \sim t$ with a prefactor that is independent of U, while for $t \gtrsim 0.5/t_0$, the time dependence crosses over to a linear increase with a strongly U-dependent slope. Plotting $S_{\rm vN}$ versus t/U results in a collapse of the data [see the inset in Fig. 4], comparable to the behavior of the staggered magnetization.

The prefactor c_s of the linear increase of the von Neumann entropy is related to the existence of gapless modes and given by the characteristic velocities [44]. We have extracted the

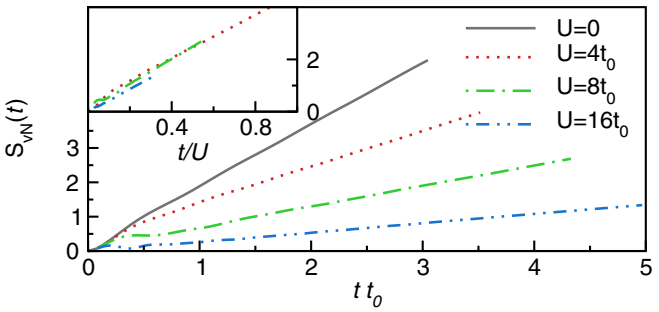

FIG. 4. (Color online) Von Neumann entropy $S_{\rm vN}$ for a central cut through the system as a function of time for $U/t_0 = 0,4,8,16$ (iTEBD results). Inset: $S_{\rm vN}$ plotted versus t/U for $U/t_0 = 4,8,16$.

prefactor of $S_{\rm vN}$ from the increase in the U-dependent regime, shown in Fig. 5. It turns out to be a monotonically decreasing function of U/t_0. We further compare c_s to the exact value of the spinon velocity $v_s^{\rm BA}$ known from the Bethe ansatz [69–71] (dashed line in Fig. 5):

$$v_s^{\rm BA} = 2t_0 \frac{I_1(2\pi t_0/U)}{I_0(2\pi t_0/U)} \tag{9}$$

(I_0 and I_1 are modified Bessel functions of the first kind). Both c_s and $v_s^{\rm BA}$ clearly have a very similar dependence on U/t_0, unambiguously showing that the long-time dynamics of the entanglement entropy are controlled by spin excitations.

B. Time averages of double occupancy

In the analysis of time averages, it is instructive to compare them to the expectation values in the diagonal and canonical ensemble. The diagonal ensemble is defined as [45]

$$O_{\rm diag} = \sum_\alpha |c_\alpha|^2 \langle\alpha|\hat{O}|\alpha\rangle, \tag{10}$$

where $|\alpha\rangle$ are postquench eigenstates ($H|\alpha\rangle = E_\alpha|\alpha\rangle$) and $c_\alpha = \langle\psi_0|\alpha\rangle$ are the overlaps between the initial state and postquench eigenstates. $O_{\rm diag}$ is the long-time average of $\langle\hat{O}\rangle$ [45], where degeneracies do not enter.

Given that the double occupancy can routinely be measured in quantum gas experiments [21,37], we concentrate the

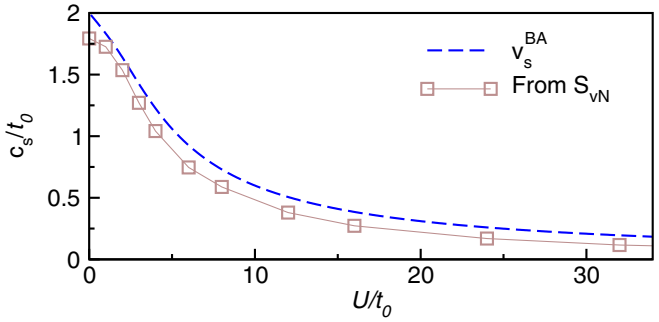

FIG. 5. (Color online) Characteristic velocities c_s extracted from the time dependence of the von Neumann entropy $S_{\rm vN}$ in the U-dependent regime $t \gtrsim 0.5/t_0$, plotted versus U/t_0 (circles). For comparison we include the exact values $v_s^{\rm BA}$ (dashed line) of the spin velocity known from the Bethe-ansatz solution [69].

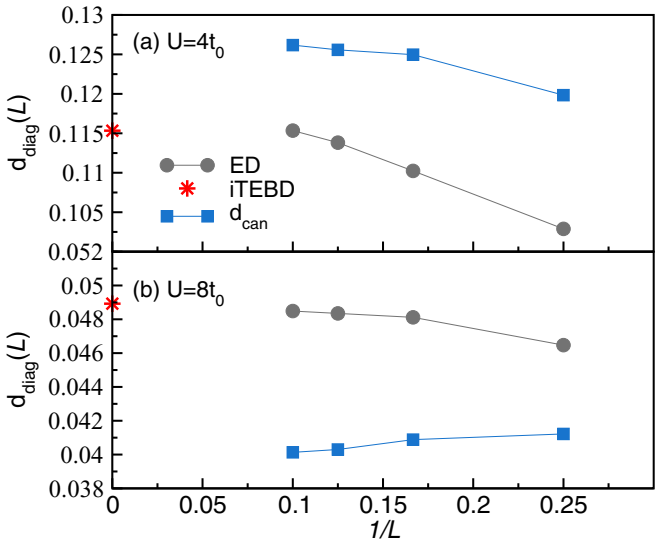

FIG. 6. (Color online) Finite-size scaling of the expectation value of the double occupancy in the diagonal ensemble (circles) $d_{\rm diag}$ for (a) $U = 4t_0$ and (b) $U = 8t_0$ (circles, ED data for $L = 4,6,8,10$; star, time average $\bar{d}$ from iTEBD). The expectation values in the canonical ensemble, $d_{\rm can}$, are also included (squares).

following discussion on this quantity. The values for $d_{\rm diag}$ computed for $L = 10$ using ED are included in Fig. 1(a) as dashed lines. Clearly, the time-dependent iTEBD data are very close to $d_{\rm diag}$ and seem to approach this value as the amplitude of oscillations decays.

To get a feeling for the system-size dependence, we show $d_{\rm diag}$ versus $1/L$ for (a) $U = 4t_0$ and (b) $U = 8t_0$, together with $\bar{d}$ extracted from iTEBD simulations plotted at $1/L = 0$ in Figs. 6(a) and 6(b), respectively. The finite-size dependence of the data for $d_{\rm diag}$ is consistent with $d_{\rm diag}(L) \to \bar{d}$ as system size increases. We should stress, though, that the time average of the double occupancy itself could change if we were able to reach longer times with the iTEBD approach.

The expectation value in the canonical ensemble is computed from

$$O_{\rm can} = {\rm tr}[\rho \hat{O}], \tag{11}$$

where $\rho = \exp(-\beta H)/Z$ with Z the partition function, all evaluated at fixed $N = L$ and vanishing total spin $\sum_{i=1}^{L} \langle S_i^z \rangle = 0$. The temperature $T = 1/\beta$ is fixed by requiring that

$$E = \langle \psi_0 | H | \psi_0 \rangle = {\rm tr}[\rho H]. \tag{12}$$

While in our problem $E = 0$, independently of the postquench value of U, the canonical temperature T clearly is a function of U/J since the postquench ground-state energy $E_{\rm gs}(U)$, defining for each U/J the zero-temperature reference point, depends on U/J. To illustrate this point, we introduce the *excess* energy

$$\delta E = E - E_{\rm gs}(U). \tag{13}$$

The canonical temperature T/U expressed in units of U and the excess energy δE are plotted versus U/J in the main panel and inset of Fig. 7, respectively. Both T/U and δE are monotonously increasing functions of U/J as U/J is lowered.

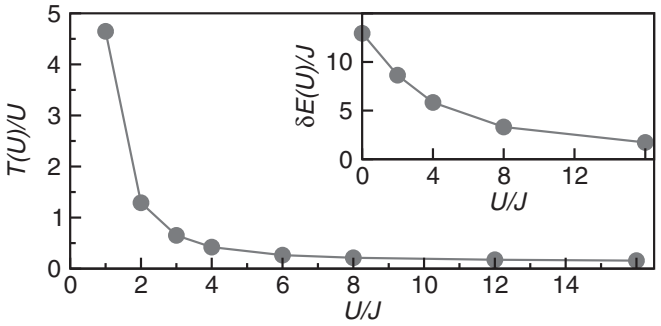

FIG. 7. Canonical temperature T/U (main panel) and excess energy δE [see Eqs. (12) and (13)] versus U/J for $L = 10$ (ED results).

At $U/J = \infty$, δE is zero since the initial state is in the ground-state manifold in that limit. As U/J decreases, $E = 0$ moves towards the middle of the many-body spectrum (see also the discussion in Sec. III C 2 and Fig. 9) and eventually, at $U = 0$, it translates into an infinite temperature (see also Ref. [72]). It is thus more appropriate to express T in units of U rather than J in the large-U/J regime since this results in $T/U \to 0$ for $U/J \to \infty$ [72].

From the time-dependent data shown in Fig. 1(a), we extract the time averages $\bar{d}$ of the double occupancy. These are displayed in Fig. 8(a) versus U/t_0 (circles) together with the expectation values $d_{\rm gs}$ in the ground state (triangles, DMRG data) and the expectation value $d_{\rm can}$ in the canonical ensemble (stars). First, we observe that, as anticipated from Fig. 1(a), $\bar{d} \approx d_{\rm diag}$ for the accessible time scales or system sizes [data for $d_{\rm diag}$ not shown in Fig. 8(a)].

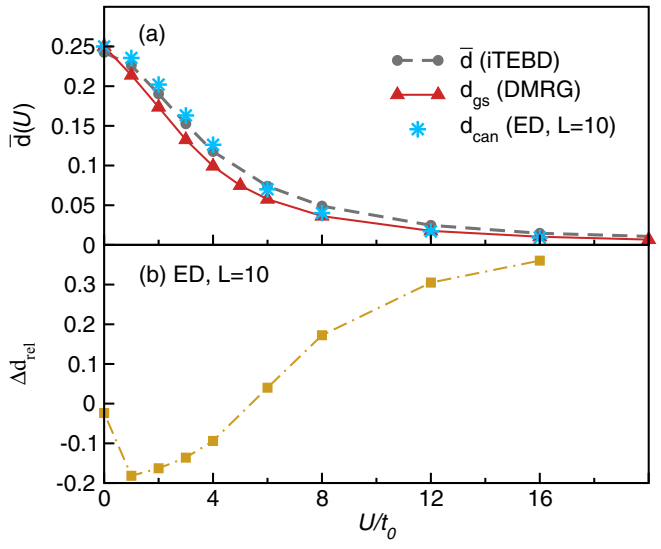

FIG. 8. (Color online) (a) Time averages (circles) of the double occupancy as a function of U/t_0. Time averages are obtained by averaging over full periods of the oscillations. Triangles denote the ground-state expectation values (computed with DMRG for $L = 64$ and open boundary conditions) for comparison; stars are the expectation values in the canonical ensemble Eq. (11) computed with ED for $L = 10$. (b) Relative difference between canonical and diagonal ensemble $\Delta d_{\rm rel} = (d_{\rm diag} - d_{\rm can})/d_{\rm diag}$.

Second, the time averages are *above* the ground-state expectation values. This behavior is, in the large-U/t_0 limit, somewhat unexpected, given the known nonmonotonic temperature dependence of d. As a function of T, the equilibrium double occupancy $d(T)$ first decreases from its zero-temperature value and then increases for large T towards $d(T=\infty)=1/4$ (see Refs. [73,74]). The position of the minimum in $d(T)$ can be interpreted as a scale for the separation of the spin- versus charge-excitation-dominated temperature regime. Since we do not observe $\bar{d} < d_{\mathrm{gs}}$ up to $U/t_0 = 64$, we conclude that the initial state always mixes in doublons from the upper Hubbard band and not just the virtual doublons present in the ground state. For the accessible system sizes, this is confirmed by the discussion presented in Sec. III C.

We further observe the known $d_{\mathrm{gs}} \propto 1/U^2$ behavior [75,76] in the large-U/t_0 regime (also obeyed by $\bar{d}$). The value of $d = 1/4$, which is the infinite-temperature expectation value at $U = 0$, is approached by $\bar{d}$ and d_{diag} as U/t_0 is lowered (see Fig. 8).

Since the system is integrable, it is not surprising that the expectation values in the canonical ensemble are different from the ones in the diagonal ensemble. The canonical ensemble has been computed for a small system using exact diagonalization, and, therefore, a quantitative comparison only makes sense by comparing to the diagonal ensemble but not to the iTEBD time averages. The relative difference is shown in Fig. 8(b) for $L = 10$ and can be quite large. At least for the accessible system sizes (see Fig. 6), this difference does not seem to become smaller. Therefore, we do not observe thermalization in this model for the quench protocol studied here. Nonetheless, the qualitative dependence of $\bar{d}$, d_{can}, and d_{diag} on U/t_0 is quite similar.

C. Connection to eigenstate thermalization hypothesis

1. Eigenstate expectation values

One popular framework to understand thermalization in closed many-body systems is the eigenstate thermalization hypothesis (ETH) [45–47]. It states that $O_{\mathrm{diag}} = O_{\mathrm{mc}}$, where O_{mc} is the expectation value in the microcanonical ensemble, if the expectation values $\langle\alpha|\hat{O}|\alpha\rangle$ of $\hat{O}$ (a local observable) in postquench eigenstates only depend on energy E in the thermodynamic limit (the latter also assuming a narrow initial state [45,72]). In other words, expectation values computed in a typical many-body eigenstate (which should be the vast majority of all states) already yield thermal behavior. For sufficiently large systems, expectation values in the microcanonical and canonical ensembles should agree with each other.

On a finite system accessible to exact diagonalization, validity of the ETH manifests itself in a narrow width of $\langle\alpha|\hat{O}|\alpha\rangle$ at a fixed energy E for a generic quantum system, while for a 1D integrable system, $\langle\alpha|\hat{O}|\alpha\rangle$ can be very broad for a given energy, due to the existence of many nontrivial (local) conservation laws resulting in a large fraction of degeneracies. The picture has been studied and often verified (see, e.g., Refs. [45,48,49,52,77–81]), the important question being how quickly the distributions of $\langle\alpha|\hat{O}|\alpha\rangle$ become sufficiently narrow as system size increases. Recent work suggests that for a generic system this is exponentially fast in L [82] (see also Refs. [72,83]), while for an integrable system, the decay of the width of $\langle\alpha|\hat{O}|\alpha\rangle$ at a given E is at most a power-law decay [82,84,85] (see also Ref. [86]).

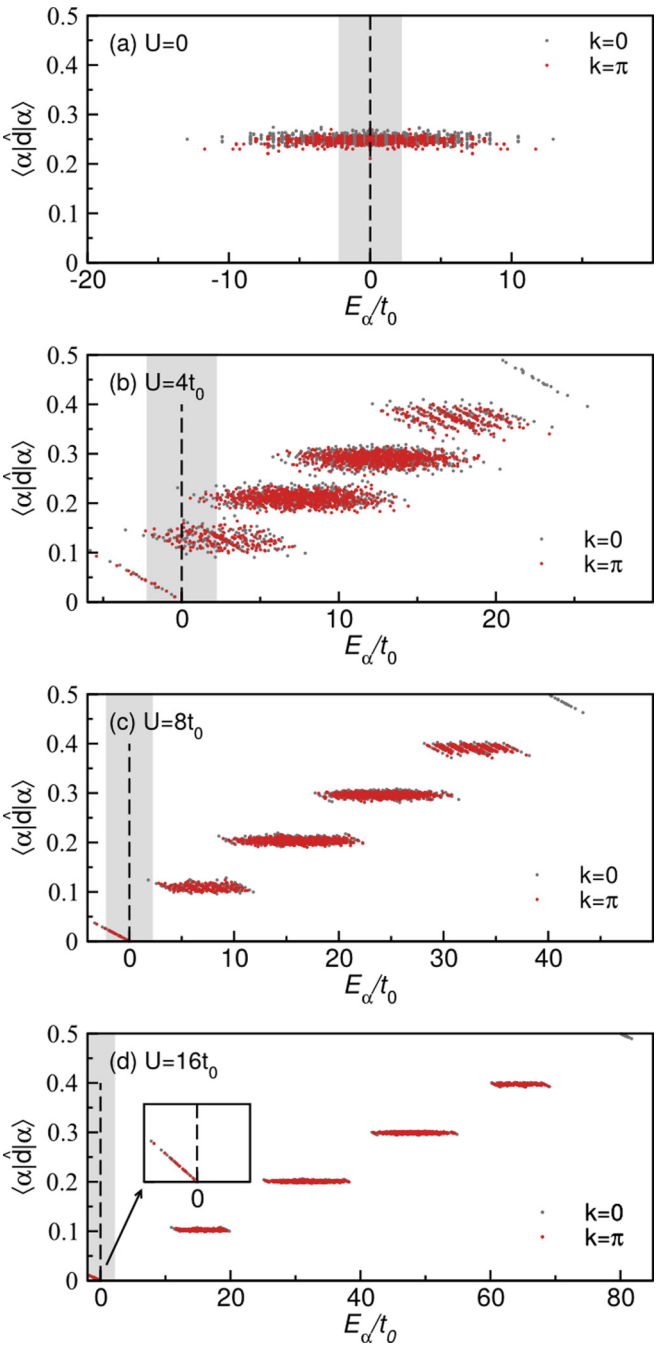

FIG. 9. (Color online) Postquench eigenstate expectation values for the double occupancy for various interaction strengths: (a) $U/t_0 = 0$, (b) $U/t_0 = 4$, (c) $U/t_0 = 8$, and (d) $U/t_0 = 16$ (ED data for $L = 10$). The vertical dashed lines mark the quench energy $E = 0$ for our initial state. The inset in (d) shows a blow-up of the first doublon band. The Néel state is doubly degenerate (denoted by $|\psi_0\rangle$ and $|\tilde{\psi}_0\rangle$) and the linear combinations $|\psi_\pm\rangle = (|\psi_0\rangle \pm |\tilde{\psi}_0\rangle)/\sqrt{2}$ live in the total quasimomentum $k = 0$ and $k = \pi$ subspaces.

Here, we exclusively analyze the distribution of postquench eigenstate-expectation values of the double occupancy. These are presented in Figs. 9(a)–9(d) for $U/t_0 = 0,4,8,16$. For

$U/t_0 \gtrsim 4$, the distributions have a very regular structure inherited from the $U/t_0 = \infty$ limit, where the double occupancy is a conserved quantity. There is one band for each possible value of $\langle\alpha|\hat{d}|\alpha\rangle$ (for the parameters of the figure, $L = 10$, these are $L\langle\alpha|\hat{d}|\alpha\rangle = 0,1,2,3,4,5$). For a nonzero and small t_0/U, the exact degeneracy in these bands is lifted while the structure as such is preserved on these small systems. In the lowest band, the effect of $t_0 \neq 0$ is to lower the energy from the degenerate $U/t_0 = \infty$ ground-state manifold at $E = 0$ towards the correlated ground state, resulting at the same time in an *increase* of $\langle\alpha|\hat{d}|\alpha\rangle$ towards its nonzero ground-state expectation value. This lowest band is very sharp and its negative slope translates into the decrease of $d = d(T)$ from its zero-temperature value as a function of temperature at low T [73,74], which persists as long as the $dL = 0$ band remains well separated from the $dL = 1$ band.

At smaller U/t_0, the bands eventually start to overlap and they become very broad at a fixed energy (compare the discussion in Refs. [78,87] for other models). At $U = 0$, the distribution of $\langle\alpha|\hat{d}|\alpha\rangle$ becomes flat, resulting in an essentially energy-independent mean value of $\langle\alpha|\hat{d}|\alpha\rangle \approx 1/4$.

2. *Properties of the specific initial state*

Our initial state has a mean energy of $E = 0$ and a width (in the diagonal ensemble) of $\sigma_{\text{diag}} = \sqrt{\langle\psi_0|H^2|\psi_0\rangle} = t_0\sqrt{2L}$, which is independent of U. This is indicated by the shaded areas in Fig. 9. For large U/t_0, primarily the very narrow first band is sampled and $E = 0$ sits at the high-energy edge of the first, $dL = 0$ band (recall that for $U/t_0 = \infty$, dL takes integer values). Therefore, the initial state asymmetrically mixes in eigenstates with too-large values of $\langle\alpha|\hat{d}|\alpha\rangle$ first from states in the $dL = 0$ band at $E < 0$, and second, from the band with $dL = 1$ (the latter follows from analyzing the distribution of $|c_\alpha|^2$). Hence, the overall structure of the distribution of $\langle\alpha|\hat{d}|\alpha\rangle$ combined with the distribution of $|c_\alpha|^2$ is consistent with the observation that $\bar{d} > d_{\text{can}}$ at large U/t_0 (compare Sec. III B).

At very small U/t_0, the initial state samples the bulk of the system where the density of states is large. At $U = 0$, the corresponding canonical temperature derived from the quench energy is infinite and since $\langle\alpha|\hat{d}|\alpha\rangle$ does not depend much on energy, we must find $\bar{d} = d_{\text{diag}} = d_{\text{can}} \to 1/4$ as L increases, consistent with the discussion in Sec. III B. At intermediate U/t_0, the initial state samples several overlapping and partially very broad bands of the $\langle\alpha|\hat{d}|\alpha\rangle$ distribution [see, e.g., the case of $U/t_0 = 4$ shown in Fig. 9(b)]. Therefore, based on the structure of the eigenstate-expectation-value distributions at the quench energy, we expect deviations between thermal behavior at intermediate and large U/J, consistent with our previous analysis. In conclusion, we stress that the quench energy alone is not a sufficient criterion for the analysis of finite-system size data, but that the actual distribution of overlaps $|c_\alpha|^2$ crucially determines which bands are involved (see also the discussion in Ref. [72]).

IV. SUMMARY AND CONCLUSION

In this work, we studied the relaxation dynamics in the one-dimensional Fermi-Hubbard model starting from a perfect Néel state as a function of the interaction strength U/t_0. As a main result, we reported evidence that the relaxation dynamics of the staggered moment, spin correlations and of the von Neumann entropy at long times is controlled by spin excitations, while the double occupancy undergoes a much faster dynamics controlled by charge excitations. The slope c_s of the increase of the von Neumann entropy $S_{\text{vN}} = c_s t$ is very similar to the exact spinon velocity known from the Bethe ansatz. This separation of time scales for double occupancy versus staggered magnetization could be accessible in state-of-the-art quantum gas experiments.

We further demonstrated that the time averages of the double occupancy are different from the expectation values in the canonical ensemble. Nonetheless, both quantities exhibit the same qualitative dependence on U/t_0. Finally, we made a connection to the eigenstate thermalization hypothesis by showing that the eigenstate expectation values of the double occupancy are, in general, broadly distributed with no well-defined dependence on energy only, characteristic for an integrable one-dimensional system.

ACKNOWLEDGMENTS

We thank F. Essler, M. Rigol, U. Schneider, D. Schuricht, and L. Vidmar for helpful discussions. F.D. and F.H.-M. acknowledge support from the Deutsche Forschungsgemeinschaft (DFG) via Research Unit FOR 1807 through Grant No. HE 5242/3-1.

[1] H.-J. Miesner, D. Stamper-Kurn, M. Andrews, D. Durfee, S. Inouye, and W. Ketterle, Science **279**, 1005 (1998).
[2] R. P. Smith, S. Beattie, S. Moulder, R. L. D. Campbell, and Z. Hadzibabic, Phys. Rev. Lett. **109**, 105301 (2012).
[3] S. Braun, M. Friesdorf, S. Hodgman, M. Schreiber, J. Ronzheimer, A. Riera, M. del Rey, I. Bloch, J. Eisert, and U. Schneider, Proc. Natl. Acad. Sci. USA **112**, 3641 (2015).
[4] P. Werner, N. Tsuji, and M. Eckstein, Phys. Rev. B **86**, 205101 (2012).
[5] N. Tsuji, M. Eckstein, and P. Werner, Phys. Rev. Lett. **110**, 136404 (2013).
[6] P. Barmettler, M. Punk, V. Gritsev, E. Demler, and E. Altman, Phys. Rev. Lett. **102**, 130603 (2009).
[7] P. Barmettler, M. Punk, V. Gritsev, E. Demler, and E. Altman, New J. Phys. **12**, 055017 (2010).
[8] M. Brockmann, B. Wouters, D. Fioretto, J. D. Nardis, R. Vlijm, and J.-S. Caux, J. Stat. Mech. (2014) P12009.
[9] W. Liu and N. Andrei, Phys. Rev. Lett. **112**, 257204 (2014).
[10] M. Heyl, Phys. Rev. Lett. **113**, 205701 (2014).

[11] M. Fagotti, M. Collura, F. H. L. Essler, and P. Calabrese, Phys. Rev. B **89**, 125101 (2014).
[12] B. Wouters, J. De Nardis, M. Brockmann, D. Fioretto, M. Rigol, and J.-S. Caux, Phys. Rev. Lett. **113**, 117202 (2014).
[13] B. Pozsgay, M. Mestyan, M. A. Werner, M. Kormos, G. Zarand, and G. Takacs, Phys. Rev. Lett. **113**, 117203 (2014).
[14] E. J. Torres-Herrera, M. Vyas, and L. F. Santos, New J. Phys. **16**, 063010 (2014).
[15] M. Rigol, V. Dunjko, V. Yurovsky, and M. Olshanii, Phys. Rev. Lett. **98**, 050405 (2007).
[16] S. Wall, D. Brida, S. R. Clark, H. P. Ehrke, D. Jaksch, A. Ardavan, S. Bonora, H. Uemura, Y. Takahashi, T. Hasegawa, H. Okamoto, G. Cerullo, and A. Cavalleri, Nat. Phys. **7**, 114 (2011).
[17] H. Ehrke, R. I. Tobey, S. Wall, S. A. Cavill, M. Först, V. Khanna, T. Garl, N. Stojanovic, D. Prabhakaran, A. T. Boothroyd, M. Gensch, A. Mirone, P. Reutler, A. Revcolevschi, S. S. Dhesi, and A. Cavalleri, Phys. Rev. Lett. **106**, 217401 (2011).
[18] L. Rettig, R. Cortés, S. Thirupathaiah, P. Gegenwart, H. S. Jeevan, M. Wolf, J. Fink, and U. Bovensiepen, Phys. Rev. Lett. **108**, 097002 (2012).
[19] S. Trotzky, Y.-A. Chen, A. Flesch, I. P. McCulloch, U. Schollwöck, J. Eisert, and I. Bloch, Nat. Phys. **8**, 325 (2012).
[20] M. Cheneau, P. Barmettler, D. Poletti, M. Endres, P. Schauß, T. Fukuhara, C. Gross, I. Bloch, C. Kollath, and S. Kuhr, Nature (London) **481**, 484 (2012).
[21] J. P. Ronzheimer, M. Schreiber, S. Braun, S. S. Hodgman, S. Langer, I. P. McCulloch, F. Heidrich-Meisner, I. Bloch, and U. Schneider, Phys. Rev. Lett. **110**, 205301 (2013).
[22] T. Fukuhara, A. Kantian, M. Endres, M. Cheneau, P. Schauß, S. Hild, C. Gross, U. Schollwöck, T. Giamarchi, I. Bloch, and S. Kuhr, Nat. Phys. **9**, 235 (2013).
[23] T. Fukuhara, P. Schauß, M. Endres, S. Hild, M. Cheneau, I. Bloch, and C. Gross, Nature (London) **502**, 76 (2013).
[24] D. Pertot, A. Sheikhan, E. Cocchi, L. A. Miller, J. E. Bohn, M. Koschorreck, M. Köhl, and C. Kollath, Phys. Rev. Lett. **113**, 170403 (2014).
[25] R. C. Brown, R. Wyllie, S. B. Koller, E. A. Goldschmidt, M. Foss-Feig, and J. V. Porto, Science **348**, 540 (2015).
[26] S. Hild, T. Fukuhara, P. Schauß, J. Zeiher, M. Knap, E. Demler, I. Bloch, and C. Gross, Phys. Rev. Lett. **113**, 147205 (2014).
[27] D. McKay and B. DeMarco, Rep. Prog. Phys. **74**, 054401 (2011).
[28] L. De Leo, C. Kollath, A. Georges, M. Ferrero, and O. Parcollet, Phys. Rev. Lett. **101**, 210403 (2008).
[29] M. Lubasch, V. Murg, U. Schneider, J. I. Cirac, and M.-C. Bañuls, Phys. Rev. Lett. **107**, 165301 (2011).
[30] W. Yi, S. Diehl, A. J. Daley, and P. Zoller, New J. Phys. **14**, 055002 (2012).
[31] T. Barthel, C. Kasztelan, I. P. McCulloch, and U. Schollwöck, Phys. Rev. A **79**, 053627 (2009).
[32] R. Jördens, N. Strohmaier, K. Günter, H. Moritz, and T. Esslinger, Nature (London) **455**, 204 (2008).
[33] U. Schneider, L. Hackermüller, S. Will, T. Best, I. Bloch, T. A. Costi, R. W. Helmes, D. Rasch, and A. Rosch, Science **322**, 1520 (2008).
[34] J. H. Jasper S. Krauser, S. G. Nick Fläschner, O. Jürgensen, D.-S. Lühmann, C. Becker, and K. Sengstock, Nat. Phys. **8**, 813 (2012).
[35] D. Greif, T. Uehlinger, G. Jotzu, L. Tarruell, and T. Esslinger, Science **340**, 1307 (2013).
[36] R. A. Hart, P. M. Duarte, T.-L. Yang, X. Liu, T. Paiva, E. Khatami, R. T. Scalettar, N. Trivedi, D. A. Huse, and R. G. Hulet, Nature (London) **519**, 211 (2015).
[37] N. Strohmaier, D. Greif, R. Jördens, L. Tarruell, H. Moritz, T. Esslinger, R. Sensarma, D. Pekker, E. Altman, and E. Demler, Phys. Rev. Lett. **104**, 080401 (2010).
[38] S. Will, D. Iyer, and M. Rigol, Nat. Commun. **6**, 6009 (2015).
[39] M. Schreiber, S. S. Hodgman, P. Bordia, H. P. Lüschen, M. H. Fischer, R. Vosk, E. Altman, U. Schneider, and I. Bloch, arXiv:1501.05661.
[40] G. Vidal, Phys. Rev. Lett. **98**, 070201 (2007).
[41] T. Giamarchi, *Quantum Physics in One Dimension* (Clarendon Press, Oxford, 2004), p. 2905.
[42] G. D. Chiara, S. Montangero, P. Calabrese, and R. Fazio, J. Stat. Mech.: Theory Exp. (2006) P03001.
[43] A. Läuchli and C. Kollath, J. Stat. Mech.: Theory Exp. (2008) P05018.
[44] P. Calabrese and J. Cardy, J. Stat. Mech.: Theory Exp. (2007) P06008.
[45] M. Rigol, V. Dunjko, and M. Olshanii, Nature (London) **452**, 854 (2008).
[46] M. Srednicki, Phys. Rev. E **50**, 888 (1994).
[47] J. M. Deutsch, Phys. Rev. A **43**, 2046 (1991).
[48] M. Rigol, Phys. Rev. A **80**, 053607 (2009).
[49] L. F. Santos and M. Rigol, Phys. Rev. E **81**, 036206 (2010).
[50] M. Kollar and M. Eckstein, Phys. Rev. A **78**, 013626 (2008).
[51] S. Genway, A. F. Ho, and D. K. K. Lee, Phys. Rev. Lett. **105**, 260402 (2010).
[52] S. Genway, A. F. Ho, and D. K. K. Lee, Phys. Rev. A **86**, 023609 (2012).
[53] S. A. Hamerla and G. S. Uhrig, Phys. Rev. B **87**, 064304 (2013).
[54] D. Iyer, R. Mondaini, S. Will, and M. Rigol, Phys. Rev. A **90**, 031602 (2014).
[55] L. Riegger, G. Orso, and F. Heidrich-Meisner, Phys. Rev. A **91**, 043623 (2015).
[56] F. Queisser, K. V. Krutitsky, P. Navez, and R. Schützhold, Phys. Rev. A **89**, 033616 (2014).
[57] L. Vidmar, S. Langer, I. P. McCulloch, U. Schneider, U. Schollwöck, and F. Heidrich-Meisner, Phys. Rev. B **88**, 235117 (2013).
[58] S. R. White, Phys. Rev. Lett. **69**, 2863 (1992).
[59] U. Schollwöck, Rev. Mod. Phys. **77**, 259 (2005).
[60] U. Schollwöck, Ann. Phys. (N. Y.) **326**, 96 (2011).
[61] A. Daley, C. Kollath, U. Schollwöck, and G. Vidal, J. Stat. Mech.: Theory Exp. (2004) P04005.
[62] S. R. White and A. E. Feiguin, Phys. Rev. Lett. **93**, 076401 (2004).
[63] G. Vidal, Phys. Rev. Lett. **93**, 040502 (2004).
[64] S. R. Manmana, A. Muramatsu, and R. M. Noack, AIP Conf. Proc. **789**, 269 (2005).
[65] A. Sheikhan and C. Kollath, Phys. Rev. A **91**, 043611 (2015).
[66] M. Rigol, A. Muramatsu, and M. Olshanii, Phys. Rev. A **74**, 053616 (2006).
[67] M. Cramer, A. Flesch, I. P. McCulloch, U. Schollwöck, and J. Eisert, Phys. Rev. Lett. **101**, 063001 (2008).
[68] P. Fazekas, *Lecture Notes on Electron Correlations and Magnetism* (World Scientific, Singapore, 1999).
[69] M. Takahashi, Prog. Theor. Phys. **43**, 1619 (1970).
[70] R. Preuss, A. Muramatsu, W. von der Linden, P. Dieterich, F. F. Assaad, and W. Hanke, Phys. Rev. Lett. **73**, 732 (1994).

[71] F. Essler, H. Frahm, F. Göhmann, A. Klümper, and V. E. Korepin, *The One-Dimensional Hubbard Model* (Cambridge University Press, Cambridge, U.K., 2005).
[72] S. Sorg, L. Vidmar, L. Pollet, and F. Heidrich-Meisner, Phys. Rev. A **90**, 033606 (2014).
[73] E. V. Gorelik, I. Titvinidze, W. Hofstetter, M. Snoek, and N. Blümer, Phys. Rev. Lett. **105**, 065301 (2010).
[74] E. V. Gorelik, D. Rost, T. Paiva, R. Scalettar, A. Klümper, and N. Blümer, Phys. Rev. A **85**, 061602 (2012).
[75] H. Shiba and P. A. Pincus, Phys. Rev. B **5**, 1966 (1972).
[76] A. Pelizzola, J. Phys. A **26**, 2061 (1993).
[77] M. Rigol, Phys. Rev. Lett. **103**, 100403 (2009).
[78] M. Rigol and L. F. Santos, Phys. Rev. A **82**, 011604 (2010).
[79] G. Roux, Phys. Rev. A **81**, 053604 (2010).
[80] R. Steinigeweg, J. Herbrych, and P. Prelovšek, Phys. Rev. E **87**, 012118 (2013).
[81] H. Kim, T. N. Ikeda, and D. A. Huse, Phys. Rev. E **90**, 052105 (2014).
[82] W. Beugeling, R. Moessner, and M. Haque, Phys. Rev. E **89**, 042112 (2014).
[83] R. Steinigeweg, A. Khodja, H. Niemeyer, C. Gogolin, and J. Gemmer, Phys. Rev. Lett. **112**, 130403 (2014).
[84] T. N. Ikeda, Y. Watanabe, and M. Ueda, Phys. Rev. E **87**, 012125 (2013).
[85] V. Alba, Phys. Rev. B **91**, 155123 (2015).
[86] G. Biroli, C. Kollath, and A. M. Läuchli, Phys. Rev. Lett. **105**, 250401 (2010).
[87] L. F. Santos and M. Rigol, Phys. Rev. E **82**, 031130 (2010).